Journal of Electroceramics 2:2, 135–142, 1998

Transport Properties of the Mixed-Conducting $SrFe_{1.2}Co_{0.3}O_x$

B. MA & U. BALACHANDRAN
Energy Technology Division, Argonne National Laboratory, Argonne, Illinois 60439

Submitted July 16, 1997; Revised April 17, 1998; Accepted April 10, 1998

Abstract. Single phase $SrFe_{1.2}Co_{0.3}O_x$ sample with layered crystal structure was prepared using a solid state reaction method. Electrical conductivity and apparent oxygen diffusion coefficients of the $SrFe_{1.2}Co_{0.3}O_x$ sample were measured as functions of temperature in atmospheres of various oxygen partial pressures (P_{O_2}). Total and ionic conductivities were determined by using the conventional four-probe and electron blocking four-probe methods, respectively. The apparent oxygen diffusion coefficient was derived from the time-dependent conductivity relaxation data of the reequilibrium process after abruptly changing the P_{O_2} in the surrounding atmosphere. Several atmospheres of different P_{O_2} were established by the use of premixed gas cylinders. The conductivity of $SrFe_{1.2}Co_{0.3}O_x$ increases with increasing temperature and P_{O_2}. At 900°C in air, the total conductivity and ionic conductivity are 10 and 8 $S \cdot cm^{-2}$, respectively. The ionic transference number (≈ 0.8 in air) does not have strong temperature dependence. The activation energy increases with decreasing P_{O_2}. In air, the activation energy has a low value of ≈ 0.37 eV. The apparent oxygen diffusion coefficient was $\approx 2 \times 10^{-6}$ $cm^2 \cdot s^{-1}$ at 950°C over a wide range of P_{O_2} ($1 \leq P_{O_2} \leq 10^{-18}$ atm).

Keywords: mixed-conductor, oxygen permeation, diffusivity, ceramic membrane, Sr-Fe-Co oxide

1. Introduction

In recent years, mixed-conducting oxides have received more and more attention because of their technological importance in high-temperature electrochemical applications [1]. The Sr-Fe-Co-O systems have high electronic and oxygen ionic conductivities in both oxidizing and reducing atmospheres [2–4]. These materials have found applications in high-temperature electrodes, solid-state fuel cells, batteries, and sensors. They also hold particular promise as ceramic membranes designed to separate oxygen from air, being impervious to other gaseous constituents. It can be used to produce syngas ($CO + H_2$) by direct conversion of methane and other basic hydrocarbon gases without external electrical circuitry [5]. A schematic drawing of the methane conversion reactor is shown in Fig 1. Syngas may be used for producing high-value-added clean-burning fuels such as dimethyl ether, alcohol, and pollution-fighting fuel additives. Therefore, this material has potential for applications that will improve the economics in the next century [5–8].

When used as a ceramic membrane in a gas separation reactor, the material is exposed to large oxygen chemical potential gradients. Oxygen transports from the high-P_{O_2} side to the low-P_{O_2} side occurs if the oxygen partial pressure difference, ΔP_{O_2}, can develop a substantial oxygen flux. High oxygen permeation flux is associated with the high electronic and oxygen ionic conductivities of the membrane material. Therefore, study of its electrical transport properties is crucially important in order to understand the oxygen permeation mechanism in this material. Furthermore, it may guide us in the search for better materials to be used as oxygen-permeable dense ceramic membranes.

Phase components of the $SrFeCo_{0.5}O_x$ sample were

Fig. 1. Schematic drawing of oxygen-permeable membrane used in methane conversion reactor.

found to be sensitive to the sample preparation procedures. Detailed X-ray and neutron diffraction studies showed that $SrFeCo_{0.5}O_x$ contains a high percentage of perovskite phase [9–11]. Its multiple-phase nature led to difficulties in understanding the relationship between crystal structure and transport properties of this material. Recently, we have successfully prepared single phase $SrFe_{1.2}Co_{0.3}O_x$ material which has a layered crystal structure. In this paper, we report the conductivity of $SrFe_{1.2}Co_{0.3}O_x$ in various P_{O_2} environments, and the apparent oxygen diffusion coefficient, as determined from conductivity relaxation data. Activation energies were derived from the slopes of Arrhenius plots of conductivities. Oxygen permeation flux through membranes made of this material is estimated on the basis of our experimental data.

2. Experimental

2.1. Sample Preparation

$SrFe_{1.2}Co_{0.3}O_x$ powder was prepared using a solid state reaction method with appropriate amounts of $SrCO_3$, Fe_2O_3, and $Co(NO_3)_2 \cdot 6H_2O$ as starting chemicals; mixing and grinding was in isopropanol with zirconia media for 15 h. After drying, the mixture was calcined in air at 850°C for 16 h, with intermittent grinding. After the final calcination, the powder was ground with an agate mortar and pestle to an average size of ≈ 3 μm, and the resulting powder was pressed with a 120 MPa load into pellets of 21.5 mm diameter and ≈ 5 mm thickness. The pellets were covered by powder of the same composition to eliminate contamination and then sintered at ≈ 1200°C in air for 5 h. Subsequently, the resulting pellets were cut into thin bars with a diamond saw for four-probe conductivity experiments.

2.2. Sample Characterization

The theoretical density of $SrFe_{1.2}Co_{0.3}O_x$ was measured on the powder form samples by using an AccuPyc 1330 pycnometer and confirmed by X-ray powder diffraction. The bulk density of the samples was determined by the Archimedean method, with isopropanol as the liquid medium. Bulk density of the specimens used in our experiments was $\approx 95\%$ of the theoretical value. A scanning electron microscopy (SEM) observation on a polished surface showed no cracks or large pores in the sample. Room-temperature X-ray powder diffraction was carried out on a Scintag XRD 2000 diffractometer. Data were taken with Cu $K_{\alpha 1}$ radiation. A high-purity intrinsic Ge energy-dispersive detector was used to minimize high backgrounds due to sample fluorescence.

2.3. Conductivity Measurement

The resistance of $SrFe_{1.2}Co_{0.3}O_x$ was measured with an HP 4192A LF impedance analyzer at 23 Hz. Four platinum wires of 0.2 mm diameter were wound around the specimen to serve as probes for the total conductivity. Electron-blocking electrodes made of yttria stabilized zirconia (YSZ) were used to extract the oxygen ionic conductivity of the sample. Details on the electron-blocking electrodes were reported elsewhere [12,13]. At this low frequency, the resistance measured with an impedance analyzer was the same as that obtained with the conventional four-probe dc method. The conductivity of the specimen was calculated from its measured resistance R (in Ω) by

$$\sigma = \frac{d_{VV}}{R \cdot S} \tag{1}$$

where d_{VV} is the separation of potential probes (in cm), and S is the cross-sectional area of the specimen (in cm^2), respectively.

Figure 2 is a schematic drawing of the experimental arrangement used in our study. Environments of various P_{O_2} were achieved by using premixed gas cylinders. A *K*-type thermocouple was attached to the specimen to measure and control the temperature. During our experiments, the temperature of the specimen was controlled within 1°C. The activation energy was calculated by least-square fitting of the temperature-dependent conductivity data to following equation

$$\sigma = \frac{A}{T}\exp(-E_a/k_B T) \tag{2}$$

where A is a constant, E_a is the activation energy, k_B is the Boltzmann constant, and T is the absolute temperature.

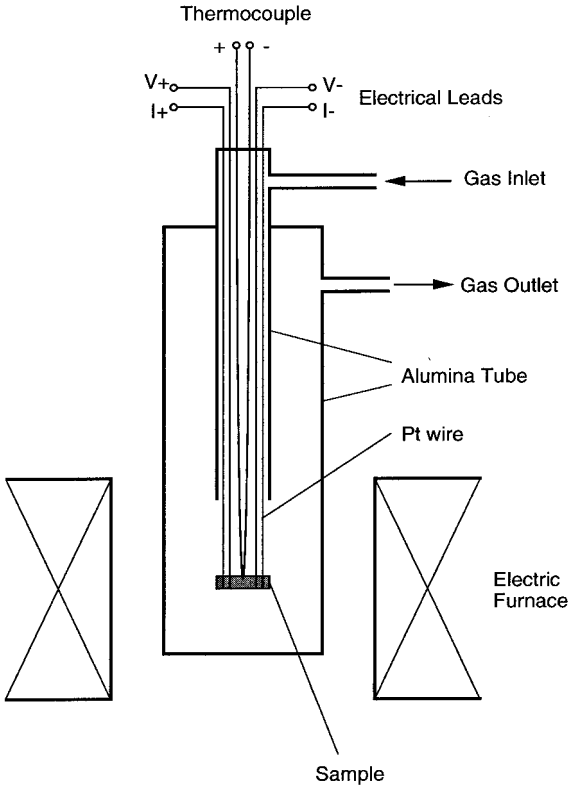

Fig. 2. Schematic drawing of experimental setup used for measuring conductivity in various atmospheres.

2.4. *Determination of Oxygen Diffusion Coefficient*

The apparent oxygen diffusion coefficient of $SrFe_{1.2}Co_{0.3}O_x$ was derived from the time-dependent conductivity relaxation method. In relaxation experiments, an abrupt change in chemical potential of one of the constituent elements (usually P_{O_2} for oxide samples) is imposed on a sample under constant temperature, and the time change of physical properties such as weight and conductivity of the sample are pursued until a new thermodynamic equilibrium state is reached. After the first proposal by Dunwald and Wagner [14], the oxygen diffusion coefficients of many oxides have been determined by the relaxation method [15–22].

When an oxide sample is subjected to a sudden change of P_{O_2} in the surrounding atmosphere, oxygen is incorporated into or released from the crystal lattice. The concentrations of various charged species in the sample will change according to the P_{O_2} of the surrounding atmosphere. During the relaxation process, oxygen nonstoichiometry spreads through the sample by lattice diffusion, which is driven by concentration gradients of defects. To carry out a conductivity relaxation experiment, the atmosphere change (specifically, the P_{O_2} gradient built up in the sample) must not be too great. Otherwise, the conducting mechanism within the sample may be different at different locations, that is, the mobility of the charge carriers would be a function of coordinates or concentration of oxygen. Then, the constant diffusion coefficient assumption would not be valid. In practice, the P_{O_2} change in the surrounding atmosphere must be large enough to allow the conductivity relaxation experiments to be carried out.

If the P_{O_2} change in the surrounding atmosphere is not too great, i.e., the conduction mechanism of the sample does not change due to the change of P_{O_2}, the time-dependent relaxation data can be used to calculate the oxygen chemical diffusion coefficient. For a thin slab specimen, the conductivity relaxation data satisfy the following equation [15]:

$$\frac{\Delta\sigma(t)}{\Delta\sigma(\infty)} = 1 - \sum_{n=0}^{\infty} \frac{8}{(2n+1)^2\pi^2}\exp\left[-\frac{(2n+1)^2\pi^2 Dt}{4l^2}\right] \tag{3}$$

where $\Delta\sigma(t) = \sigma(t) - \sigma(0)$ and $\Delta\sigma(\infty) = \sigma(\infty) - \sigma(0)$ are the changes in conductivity for the sample at time t and time infinity, respectively. D denotes the

oxygen chemical diffusion coefficient derived from the time-dependent conductivity relaxation data.

In our conductivity relaxation experiments, time to flush the system with a new gas atmosphere was several seconds, which is sufficiently short to affect the initial diffusion kinetics. To investigate the surface effect on the apparent oxygen diffusion coefficient, comparison experiments were conducted on a specimen with a different thickness. If diffusion of oxygen is limited by the surface reaction, then the apparent bulk diffusion coefficient obtained would be different for specimens with different thicknesses. However, this was not the case in our comparison experiment. At a constant temperature, the same oxygen diffusion coefficient was obtained for samples with different thickness, thus indicating that the surface reaction coefficient (sometimes also called the surface exchange coefficient) of $SrFe_{1.2}Co_{0.3}O_x$ was sufficiently high.

3. Results and Discussion

3.1. Micrographic and Crystal Structures, and Sample Density

A scanning-electron-microscopy (SEM) image of the polished surface of $SrFe_{1.2}Co_{0.3}O_x$ is shown in Fig. 3a, and an SEM image of the fracture surface is shown in Fig. 3b. These observations indicated that the $SrFe_{1.2}Co_{0.3}O_x$ sample has a dense homogeneous structure and an absence of cracks or large pores. Energy-dispersive X-ray (EDX) elemental analysis revealed that the composition of metal elements in the sample is consistent with that given in the chemical formula.

The room-temperature X-ray powder diffraction pattern is plotted in Fig. 4. This material has a layered structure. Its X-ray powder diffraction pattern can be fitted with an orthorhombic structure with lattice parameters: $a = 11.0652$, $b = 19.008$, $c = 5.5618$ Å, and volume of 1169.80 $Å^3$. There are sixteen formula compositions which exist in each unit cell. Rietveld analysis showed that the air-sintered $SrFe_{1.2}Co_{0.3}O_x$ sample is primarily a single phase material with less than 5% perovskite phase as its secondary phase [9], unlike in the air-sintered $SrFeCo_{0.5}O_x$ sample which contains about 50% perovskite phase [10,11]. Detailed discussion of the crystal structure of the sample is outside the scope of this paper and are reported elsewhere [9,23].

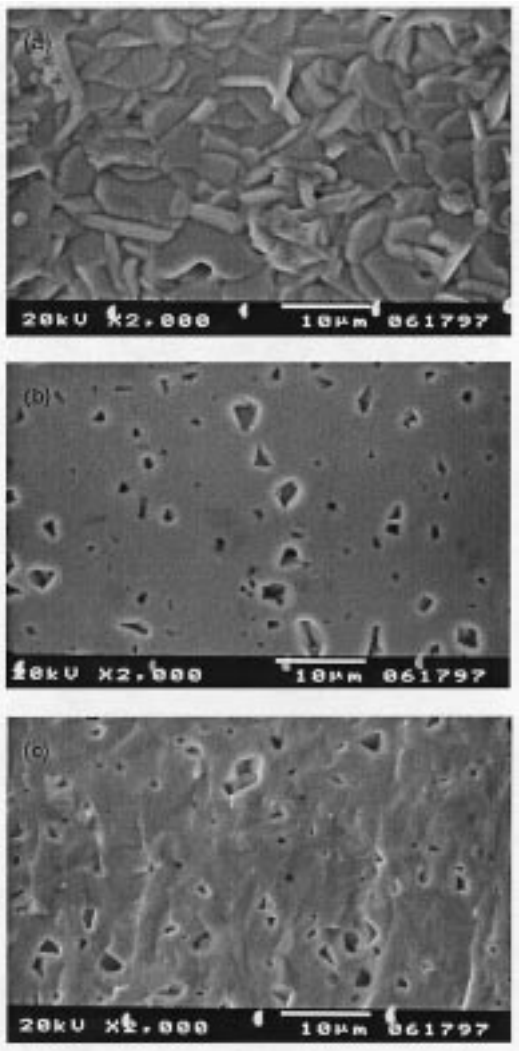

Fig. 3. SEM morphology of (*a*) as-sintered surface, (*b*) polished surface, and (*c*) fracture surface of the air- sintered $SrFe_{1.2}Co_{0.3}O_x$ sample.

The density of air- sintered $SrFe_{1.2}Co_{0.3}O_x$ sample as measured on powder with helium pycnometer is 5.088 ± 0.003 g·cm^{-3}. Powder was prepared by crushing and grinding sintered pellets using an agate mortar and pestle. The theoretical density of the sample is calculated using its chemical formula and unit cell parameters. Assuming that iron and cobalt cations exist in $+3$ and $+8/3$, respectively, in the material at room temperature in air, the oxygen content should be $x = 3.20$. Guggilla and Manthiram

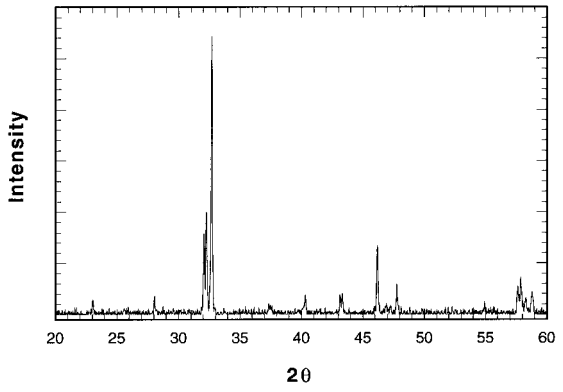

Fig. 4. Room-temperature X-ray diffraction pattern of sintered $SrFe_{1.2}Co_{0.3}O_x$ sample.

reported $x = 3.25$ in sintered $SrFe_{1.2}Co_{0.3}O_x$ samples [11]. Considering the uncertainty of oxygen content, the theoretical density of air-sintered $SrFe_{1.2}Co_{0.3}O_x$ sample determined from XRD results was $5.076 \pm 0.009\ g \cdot cm^{-3}$. The bulk density of the sample used in our experiments as determined by Archimedean method was $4.86\ g \cdot cm^{-3}$, which is $\approx 95\%$ of its theoretical value.

3.2. *Temperature- and P_{O_2}-Dependent Conductivity*

The temperature dependence of conductivities and ionic transference number of $SrFe_{1.2}Co_{0.3}O_x$ in air are shown in Fig. 5. Total, ionic, and electronic conductivities all increase with increasing temperature within the temperature range 700 to 1000°C. The oxide ionic transference number of $SrFe_{1.2}Co_{0.3}O_x$ is almost independent of temperature with a value of ≈ 0.8 at high temperature. Because the ionic transference number is a measure of the contribution from ionic conductivity to total conductivity, a value of 0.8 for the ionic transference number indicates that the ionic conductivity is about four times higher than the electronic conductivity in this material. Arrhenius plots for the total and ionic conductivities of $SrFe_{1.2}Co_{0.3}O_x$ are shown in Fig. 6. Activation energies were calculated from the slopes and indicated in the plot. Both activation energies have lower values than those of other $Sr(Fe,Co)O_x$ systems [12]. This implies that the bonding of the oxide ions to their sublattices is weak, and thus the oxide ions can move more easily in $SrFe_{1.2}Co_{0.3}O_x$ than in other $Sr(Fe,Co)O_x$ systems.

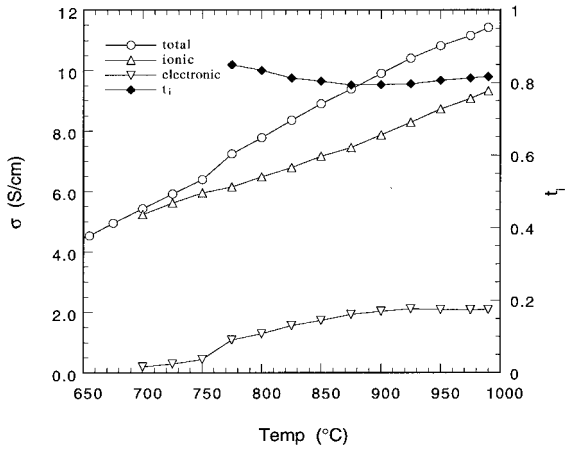

Fig. 5. Temperature-dependent conductivities (corresponding to left *y*-axis) and ionic transference number (corresponding to right *y*-axis) of sintered $SrFe_{1.2}Co_{0.3}O_x$ sample.

Figure 7 shows $\log(T\sigma)$ as a function of reciprocal temperature for $SrFe_{1.2}Co_{0.3}O_x$ in various oxygen environments. The $\log(T\sigma)$ curve has good linear dependence on reciprocal temperature. The activation energies of $SrFe_{1.2}Co_{0.3}O_x$ in various P_{O_2} environments were calculated from the slopes of these curves. The activation energies thus obtained are listed in Table 1 and plotted in Fig. 8 as a function of oxygen partial pressure. The activation energy increases with decreasing P_{O_2}, and this implies that the binding energy between oxygen ions and their sublattices becomes stronger when oxygen is moved out of the sample. The equilibrium total conductivity at 950°C is shown in Fig. 9 as a function of oxygen

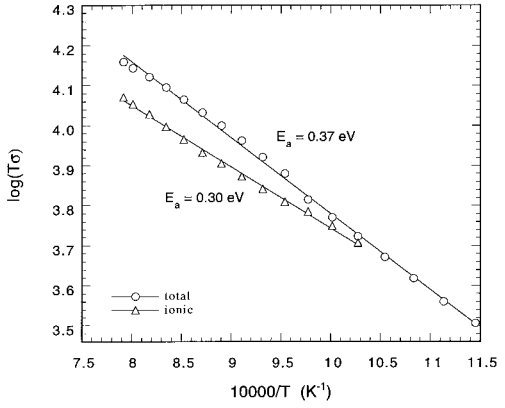

Fig. 6. Arrhenius plot for total and ionic conductivities of $SrFe_{1.2}Co_{0.3}O_x$ in air.

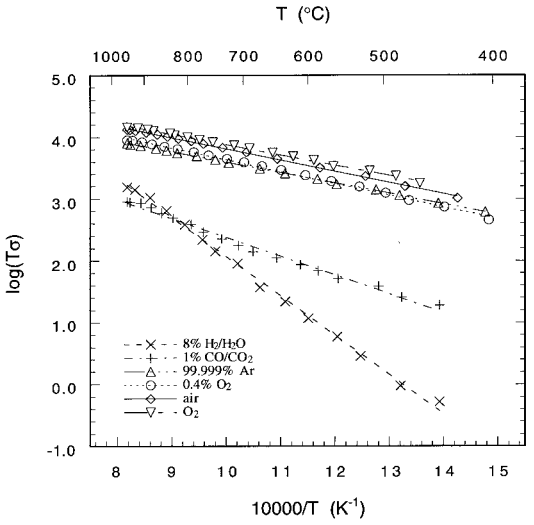

Fig. 7. Arrhenius plot for total conductivity of $SrFe_{1.2}Co_{0.3}O_x$ in various atmospheres.

partial pressure. Total conductivity decreases with decreasing P_{O_2}, and this indicates that interstitial oxygen ions exist in the sample within this P_{O_2} range [15].

3.3. Apparent Oxygen Diffusion Coefficients

The conductivity relaxation data of $SrFe_{1.2}Co_{0.3}O_x$ are shown in Fig. 10 as a function of relaxation time after switching the surrounding atmosphere. Conductivity relaxation data were analyzed by least-squares fitting to Eq. 3 with the corresponding geometric parameters of the specimens.

The apparent oxygen diffusion coefficient derived from the conductivity-relaxation data for $SrFe_{1.2}Co_{0.3}O_x$ are listed in Table 2. Compared to the results of the $SrFeCo_{0.5}O_x$ sample reported earlier [15,23], the apparent oxygen diffusion coefficient of $SrFe_{1.2}Co_{0.3}O_x$ is twice as high at 950°C in air. Since

Table 1. Conductivity at 950°C and activation energies of $SrFeCo_{0.5}O_x$ in various oxygen atmospheres

Atmosphere	$\log(P_{O_2})$	$\sigma(S \cdot cm^{-1})$	$E_a(eV)$
100% O_2	0	11.88	0.33
Air	−0.68	10.82	0.37
0.4% O_2/Ar	−2.37	7.35	0.38
99.999% Ar	−6.00	6.53	0.34
1% CO/CO_2	−11.5	0.74	0.62
8% H_2/H_2O	−18.2	1.26	1.26

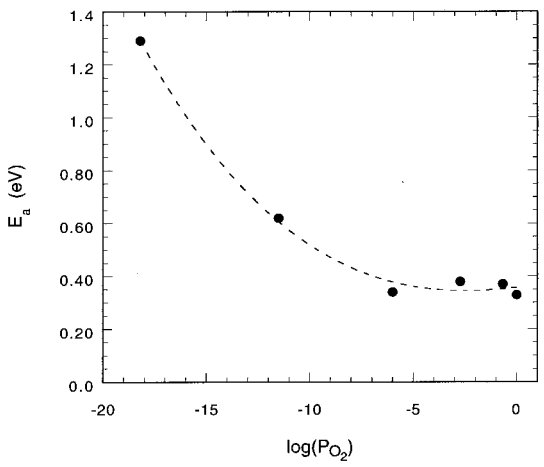

Fig. 8. Activation energy as a function of oxygen partial pressure for $SrFe_{1.2}Co_{0.3}O_x$.

the $SrFe_{1.2}Co_{0.3}O_x$ sample is primarily single phase which has layered structure, unlike the $SrFeCo_{0.5}O_x$ sample which has ≈ 50% perovskite phase, this may indicate that oxygen diffusion in the layered structure is faster than that in the perovskite structure.

3.4. Estimated Oxygen Permeability

Oxygen permeation flux through a mixed-conducting ceramic membrane of thickness L can be estimated by using its conductivity data with following equation [13]:

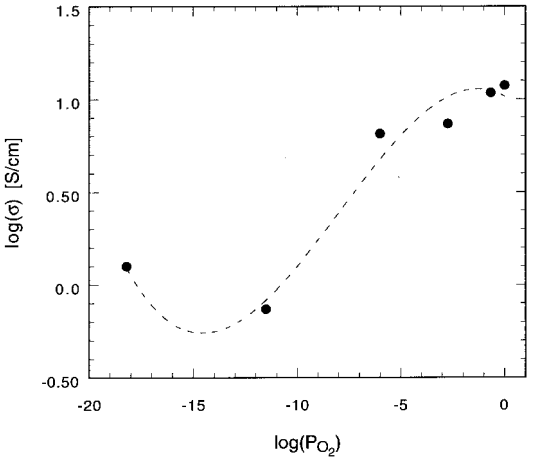

Fig. 9. Total conductivity as a function of oxygen partial pressure for $SrFe_{1.2}Co_{0.3}O_x$ at 950°C.

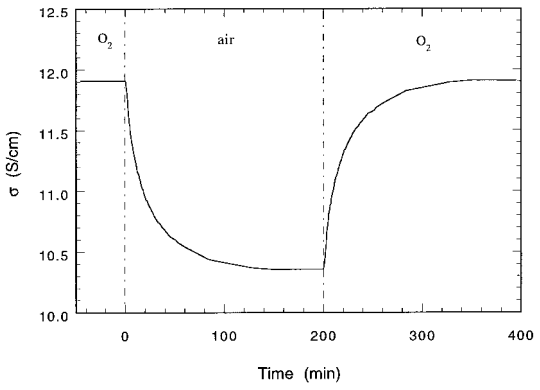

Fig. 10. Time-dependent conductivity transient behavior of $SrFe_{1.2}Co_{0.3}O_x$ at 950°C after switching surrounding atmosphere from pure oxygen to air and then back to pure oxygen.

$$J_{O_2} = -\frac{RT}{16F^2L}\cdot\overline{\sigma_{tot}t_i(1-t_i)}\cdot\ln\left(\frac{P^{II}_{O_2}}{P^{I}_{O_2}}\right) \tag{4}$$

where R is the gas constant (8.3145 $J\cdot K^{-1}\cdot mol^{-1}$), F is the Faraday's constant (9.64853×10^4 $C\cdot mol^{-1}$), and

$$\overline{\sigma_{tot}t_i(1-t_i)} = \frac{1}{\ln\left(P^{II}_{O_2}/P^{I}_{O_2}\right)} \times \int_{P^{I}_{O2}}^{P^{II}_{O2}} \sigma_{tot}t_i(1-t_i)d\ln(P_{O_2}) \tag{5}$$

is the effective permeation factor, an average of $\sigma_{tot}t_i(1-t_i)$ over the entire working P_{O_2} range. $P^{I}_{O_2}$ and $P^{II}_{O_2}$ are the oxygen partial pressures on the reference side and the reaction side, respectively. Other parameters have their usual meaning. Equation (5) tells us that the oxygen permeability of a mixed conducting oxide is controlled by ionic and electronic conduction of the material over the entire P_{O_2} range, rather than ionic or electronic conductivity alone. For a 1-mm-thick dense membrane made of $SrFe_{1.2}Co_{0.3}O_x$ material, the oxygen permeation flux at 900°C is expected to be $\approx 3\times10^{-5}$ $mol\cdot cm^{-2}\cdot s^{-1}$ or ≈ 40 $SCC/cm^2\cdot min$ when one side is exposed to air and the other side is exposed to syngas ($\Delta\log P_{O_2}\approx 20$).

Table 2. Apparent oxygen diffusion coefficients of $SrFe_{1.2}Co_{0.5}O_x$ in various oxygen atmospheres at 950°C

Atmosphere change	$\log(P_{O_2})^i$	$\log(P_{O_2})^f$	$D(cm^2\cdot s^{-1})$
Air to100% O_2	−0.68	0	2.11×10^{-6}
0.4% O_2 to air	−2.37	−0.68	3.42×10^{-6}
0.4% O_2 to 100%O_2	−2.37	0	2.19×10^{-6}
1% CO/CO_2 to 0.4% O_2	−11.1	−2.37	1.38×10^{-6}
8% H_2/H_2O to1% CO/CO_2	−18.2	−11.1	2.40×10^{-6}
100% O_2 to air	0	−0.68	2.80×10^{-6}
100% O_2 to 0.4%O_2	0	−2.37	1.47×10^{-6}
0.4% O_2 to 1% CO/CO_2	−2.37	−11.1	2.23×10^{-6}
1% CO/CO_2 to 8%H_2/H_2O	−11.1	−18.2	2.18×10^{-6}

4. Conclusions

Mixed-conducting $SrFe_{1.2}Co_{0.3}O_x$ not only exhibits electronic and oxygen ionic conductivities but also structural stability in both oxidizing and reducing atmospheres. It is a technologically important material for use in high-temperature electrochemical applications. Because of its potential high oxygen permeability at elevated temperature, it could be used as a dense ceramic membrane for separating oxygen from air.

Scanning electron microscopy showed that the sintered $SrFe_{1.2}Co_{0.3}O_x$ sample has a dense homogeneous structure without cracks or large pores. Energy-dispersive X-ray elemental analysis revealed that the composition of metal elements in the sample is consistent with that given in the chemical formula.

Conductivities of $SrFe_{1.2}Co_{0.3}O_x$ increase with increasing temperature. At 900°C in air, the total and ionic conductivities are 10 and 8 $S\cdot cm^{-1}$, respectively. Its ionic transference number, ≈ 0.8 in air, does not have a strong dependence on temperature. Conductivity increases while the activation energy decreases with increasing P_{O_2}. In high-P_{O_2} regions, the activation energy of $SrFe_{1.2}Co_{0.3}O_x$ was found to have a low value of ≈ 0.37 eV. The apparent oxygen diffusion coefficient obtained from conductivity relaxation data is $\approx 2\times10^{-6}$ $cm^2\cdot s^{-1}$ at 900°C. This is a indication that oxygen diffusion in the layered structure is faster than that in the perovskite structure.

Acknowledgment

We are grateful to Dr. J.-H. Park of Argonne National Laboratory, and to Professor C. U. Segre of the Illinois Institute of Technology for their helpful discussions. Work at Argonne National Laboratory is supported

by the U.S. Department of Energy, under Contract W-31-109-Eng-38.

References

1. H.L. Tuller, *Solid State Ionics*, **94**, 63 (1997).
2. Y. Teraoka, H.M. Zhang, S. Furnkawa, and N. Yamozoe, *Chem. Lett*., **1985**, 1743 (1985).
3. Y. Teraoka, T. Nobunaga, and N. Yamazoe, *Chem. Lett*., **1988**, 503 (1988).
4. U. Balachandran, S.L. Morissette, J.T. Dusek, R.L. Mieville, R.B. Poeppel, M.S. Kleefisch, S. Pei, T.P. Kobylinski, and C.A. Udovich, *Proc. Coal Liquefaction and Gas Conversion Contractor Review Conf*., S. Rogers et al., ed., Vol. 1, pp. 138–160, U.S. Dept. of Energy, Pittsburgh Energy Technology Center (1993).
5. U. Balachandran, T.J. Dusek, S.M. Sweeney, R.B. Poeppel, R.L. Mieville, P.S. Maiya, M.S. Kleefisch, S. Pei, T.P. Kobylinski, C.A. Udovich, and A.C. Bose, *Am. Ceram. Soc. Bull*., **74**, 71 (1995).
6. T.J. Mazanec, T.L. Cable, and J.G. Frye, Jr., *Solid State Ionics*, **53/56**, 111 (1992).
7. C. Bose, J.G. Stigel, and R.D. Srivastava, *Gas to Liquids Research Program of the U.S. Department of Energy: Programmatic Overview*, presented at Symp. on Alternative Routes for the Production of the American Chemical Society National Meeting, Washington, DC, Aug. 21–26 (1994).
8. T.L. Cable, European Patent EP 0438 902 A2, July 31 (1991).
9. J.P. Hodges, J.D. Jorgensen, D. Miller, B. Ma, U. Balachandran, and J.W. Richardson, Jr., *Mater. Res. Soc. Symp*., **496**, 173 (1998).
10. H. Fjellvag, B.C. Hauback, and R. Bredesen, *J. Mater. Chem.,* **7,** 2415 (1997).
11. S. Guggilla and A. Manthiram, *J. Electrochem. Soc*., **144**, L120 (1997).
12. B. Ma, J.-H. Park, C.U. Segre, and U. Balachandran, *Mater. Res. Soc. Symp. Proc*., **393**, 49 (1995).
13. B. Ma, U. Balachandran, J.-H. Park, and C.U. Segre, *J. Electrochem. Soc*., **143**, 1736 (1996).
14. H. Dunwald and C. Wagner, *Z. Phys. Chem*., **B24**, 53 (1934).
15. B. Ma, U. Balachandran, J.-H. Park, and C.U. Segre, *Solid State Ionics*, **83**, 65 (1996).
16. L.C. Walters and R.E. Grace, *J. Phys. Chem. Solids*, **28**, 245 (1967).
17. P.E. Childs, L.W. Laub, and J.B. Wabner, Jr., *Proc. Br. Ceram. Soc*., **19**, 29 (1971).
18. K. Kitazawa and R.L. Coble, *J. Am. Ceram. Soc*., **57**, 250 (1974).
19. R. Farhi and G. Petot-Ervas, *J. Phys Chem. Solids*, **39**, 1169 (1978).
20. C.J. Yu, D.M. Sparlin, and H.U. Anderson, *J. Am. Ceram. Soc*., **70**, C189 (1987).
21. J.-H. Park, P. Kostic, and J.P. *Singh, Mater. Letters*, **6**, 393 (1988).
22. I. Yasuda and T. Hikita, *J. Electrochem. Soc*., **141**, 1268 (1994).
23. B. Ma and U. Balachandran, *Solid State Ionics*, **100**, 53 (1997).